Direct Data-Driven Control-Based Additive Feedforward Compensation for Fast and Precise Positioning Control*

Daigo Yamaguchi[1], Shimpei Sato[1], and Yoshihiro Maeda[1]

Abstract— In industrial positioning systems where rapid response and high-precision are crucial, minor model inaccuracies due to unknown dynamics and identification errors in controller design significantly impede achieving desired positioning accuracy. This paper introduces and evaluates a novel, direct data-driven control-based additive feedforward (FF) compensation method, aimed at enhancing precision in positioning while streamlining the design process. The purpose of this additive FF compensation is to attenuate undesirable error responses resulting from modeling errors in the existing model-based FF design. The proposed method enhances control performance by utilizing data-driven prediction of positioning response and optimizing the predicted response. Moreover, this work presents a newly developed design theory for the additive FF controller and highlights its design efficiency. The effectiveness of the proposed approach is substantiated through comprehensive experiments with a galvano scanner in printed circuit board laser drilling applications, demonstrating significant improvements in positioning accuracy and response time.

I. INTRODUCTION

Productivity and processing quality requirements for industrial mechatronics, represented by electronic component processing machines and machine tools, continue to increase. In particular, the required control specifications related to the speed and accuracy of various inherent positioning mechanisms are becoming increasingly stringent[1]. In the field of fast and precise positioning control, model-based feedforward (FF) compensation based on parametric or nonparametric models of the plant is widely used, and there are many reports in literature on its effectiveness[2], [3].

The efficacy of model-based control is widely known to depend heavily on the precision of model identification. Consequently, significant research efforts have been directed not only towards controller design but also towards system identification, and advanced system identification techniques have been developed[4], [5]. However, in fast and precise positioning control, even slight errors in modeling can cause error responses that interfere with the target accuracy. In general, this makes it difficult to obtain the desired positioning performance simply by designing an FF controller using an identified model. Therefore, control engineers fine-tune the model parameters and/or introduce and adjust additive FF controllers, such as parallel type controllers[6], [7] and pre-filters[8], which requires substantial design effort. In many types of industrial machines, operating conditions are becoming more diverse, and the number of control axes is increasing. More efficient control design, which is in high demand from industry, is an important developmental challenge that will lead to lower product costs and more sophisticated control specifications.

To achieve a more efficient control design, research on data-driven control is actively being conducted[9], [10], where controllers are designed from operational data (hereinafter referred to as learning data) obtained in advance from a control system. Compared to the traditional model-based control approach, which employs a step-by-step, indirect method for control design, the data-driven control approach is expected to achieve both more efficient design processes and enhanced control performance. Among various methods, the direct data-driven control (DDC) method, which uses solely on the input/output data of a control system for learning data, is deemed the simplest and most suitable for industrial applications. This method does not require additional sensors for data acquisition and enables to directly and efficiently design controllers using learning data from a "single" operating experiment. A representative example of DDC is virtual reference feedback tuning (VRFT)[11], [12], which, as the name implies, involves designing a feedback (FB) controller by solving a control cost optimization problem for a virtual reference input. Furthermore, using a similar approach to VRFT, several methods have been proposed for designing FF controllers[13], [14], [15]. However, these DDC methods require a pre-defined reference model as a hyperparameter to generate an appropriate reference input[16]. The design process necessitates complete knowledge or an accurate model of the control system, and achieving desired control performance demands as much design effort as the model-based control approach.

In addressing the issue of reference model design in DDC, a promising strategy to improve fast and precise control performance involves the supplementary application of DDC to a traditional model-based FF control. However, to the best of our knowledge, this approach has not been explored in previous research. Therefore, the development of supplementary DDC technology, as a progressive and effective application of data-driven control, carries substantial academic importance.

In this study, to address the problem of fast and precise control of industrial positioning mechanisms, we proposed an approach to DDC-based additive FF compensation design intended to prevent degradation of positioning accuracy owing to unknown modeling errors that cannot be compen-
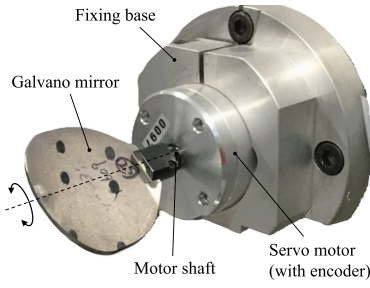
Fig. 1.   Exterior of galvano scanner.
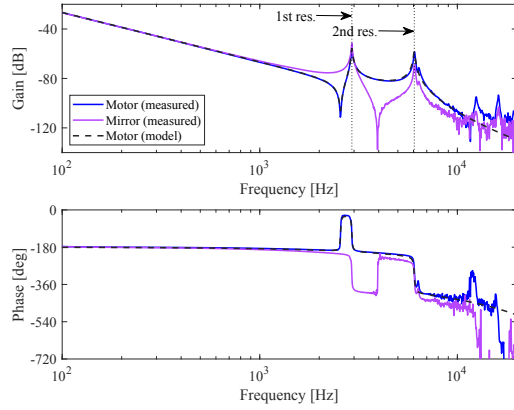
Fig. 2.   Frequency characteristics of galvano scanner.

Condition	Stroke Y_r [mrad]	Settling accuracy [µrad]	Settling time [ms]
C1	1.32	±13.2	0.48
C2	3.29	↑	0.64
C3	6.58	↑	0.72

Fig. 3.   Block diagram of two-degree-of-freedom position control system with model-based FF and additive FF.
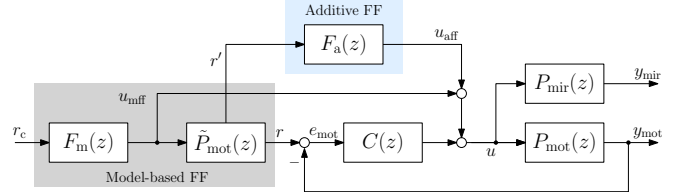
sated for via conventional model-based FF compensation. The proposed method provides an effective approach to designing an additive FF controller that predicts the response directly from learning data obtained by a single positioning experiment and solves a control cost optimization problem on the predicted response. In addition, the proposed method does not require the design of a reference model to generate a reference input by using a target reference generated by an existing model-based FF control. In this study, we newly present the design theory of the DDC-based additive FF compensation and demonstrated its effectiveness through practical positioning experiments conducted by controlling a galvano scanner in a printed circuit board laser drilling machine.

II. PROBLEM OF MODEL-BASED CONTROL APPROACH IN FAST AND PRECISE POSITIONING

A. Galvano Scanner

Fig. 1 shows an external view of the galvano scanner that served as the control target. The galvano scanner is a precise positioning mechanism for controlling the position of a laser beam in a laser drilling machine for printed circuit boards. To achieve high productivity and processing quality, a response frequency of several kHz or more and a positioning accuracy of several µm or less are required[17]. The galvano scanner is broadly composed of a galvano mirror that reflects the laser, a servo motor that drives the mirror, and a rotary encoder that detects the angular position of the motor. When driving at high acceleration or deceleration, the low rigidity of the

coupling between the motor shaft, mirror, and encoder causes resonant vibration, resulting in a deterioration in positioning accuracy. The motor is driven via a servo amplifier, and current commands (control input) to the servo amplifier are output from a digital signal processor, which performs control operations (control period $T_s = 20$ µs). The FB signal, which can be used for control operations, is the motor angular position y_{mot} detected by the encoder, resulting in a typical load resonant system under semi-closed control, where y_{mot} is used to control the angular position y_{mir} of the mirror in response to the load.

In Fig. 2, the blue lines represent the plant frequency response function (FRF) from the current command u to the motor position y_{mot} measured using the sinusoidal sweep test. The galvano scanner has a frequency characteristic with significant resonant vibration modes around 2.9 kHz and 6.0 kHz. Meanwhile, the purple lines in Fig. 2 represent the plant FRF from u to the mirror position y_{mir} detected using the position sensing device sensor. The motor and mirror positions have resonance peaks at the same frequencies, but the characteristics of each vibration mode are different.

B. Target Control Specifications

The target control specifications for three stroke conditions in Table I were examined in this study. In a point-to-point positioning operation with stroke Y_r, the motor and mirror positions must be settled to within ±13.2 µrad of the target position within each settling time. These control specifications were set considering control tuning issues under multiple typical operating conditions of galvano scanners used in industry. Challenging targets were set to achieve a high response frequency of $1.39 \sim 2.08$ kHz (defined as the reciprocal of the target settling time) for a first resonance frequency of 2.9 kHz, with high accuracy in the order of several µm at the laser irradiation position.

C. Position Control System

Fig. 3 shows a block diagram of a two-degree-of-freedom (2DoF) position control system with model-based FF and additive FF compensations. In the figure, $P_{mot}(z)$ represents

TABLE II

PARAMETERS OF PLANT MODEL $\tilde{P}_{\mathrm{mot}}(s)$.

K_{sa} [Nm/V]	3.00×10^{-3}	J [kgm^2]	1.62×10^{-6}
L [s]	29.49×10^{-6}		
ω_1 [rad/s]	$2\pi \times 2925$	ω_2 [rad/s]	$2\pi \times 6053$
ζ_1	6.77×10^{-3}	ζ_2	8.23×10^{-3}
k_1	0.40	k_2	-1.54
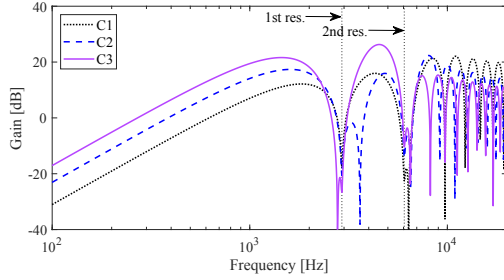
Fig. 4. Frequency characteristic of model-based FF controller $F_{\mathrm{m}}(z)$.

(a)

(b)

Fig. 5. Waveforms of model-based FF compensation: (a) position trajectory reference r; (b) model-based FF control input u_{mff}.

the dynamics of the galvano scanner to the motor position y_{mot}, $P_{\mathrm{mir}}(z)$ represents the dynamics of the galvano scanner to the mirror position y_{mir}, $C(z)$ denotes the FB controller, $\tilde{P}_{\mathrm{mot}}(z)$ is the plant model for $P_{\mathrm{mot}}(z)$, $F_{\mathrm{m}}(z)$ denotes the model-based FF controller, $F_{\mathrm{a}}(z)$ denotes the additive FF controller, r_{c} is the position command, r is the position trajectory reference to the motor, e_{mot} is the motor position tracking error, u_{mff} is the model-based FF control input, and u_{aff} is the additive FF control input. Note that the command r' input to $F_{\mathrm{a}}(z)$ is delay-free owing to the dead time factor in $\tilde{P}_{\mathrm{mot}}(z)$. If the plant model without a dead time factor is $\tilde{P}'_{\mathrm{mot}}(z)$, $r'(z) = \tilde{P}'_{\mathrm{mot}}(z)u_{\mathrm{mff}}(z)$ holds. The FB controller $C(z)$ was composed of a PID controller and two stages of second-order IIR filters connected in series. The FB controller parameters were designed in the frequency domain using the measured FRF, considering the expansion of the FB control bandwidth and robust stabilization of the first- and second-order vibration modes[19].

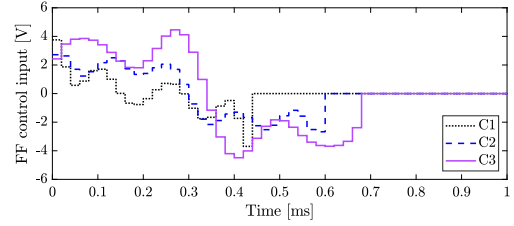### D. Design of Model-Based FF Compensation

In this study, u_{mff} and $\tilde{P}_{\mathrm{mot}}(z)$ corresponding to model-based FF compensation were designed based on deadbeat FF control manner[3]. The design model $\tilde{P}_{\mathrm{mot}}(z)$ used the following parametric model in the s-domain representation considering the two main vibration modes.

$$\tilde{P}_{\mathrm{mot}}(s) = \frac{K_{\mathrm{sa}}}{J} e^{-Ls} \left(\frac{1}{s^2} + \sum_{i=1}^{2} \frac{k_i}{s^2 + 2\zeta_i \omega_i s + \omega_i^2} \right) \quad (1)$$

where K_{sa} is the gain of servo amplifier, J is the moment of inertia, L is the equivalent dead time, ω_i is the resonance frequency of the ith vibration mode, ζ_i is the modal damping coefficient of the ith vibration mode, and k_i is the mode influence coefficient of the ith vibration mode. The model parameters were identified as shown in Table II by applying the vector fitting method[18] on the measured FRF shown by the blue lines in Fig. 2. The FRF of $\tilde{P}_{\mathrm{mot}}(z)$ obtained by
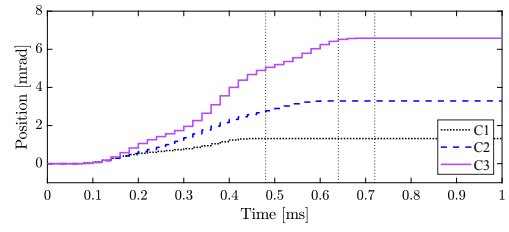
discretizing (1) via the tustin transformation with period T_{s} is represented by the black dashed lines in Fig. 2. From the figure, the identified plant model accurately reproduced the frequency response of the actual system.

The FF controller $F_{\mathrm{m}}(z)$ was designed by solving an optimization problem using $\tilde{P}_{\mathrm{mot}}(z)$ as the design model and the objective function being frequency shaping at around the first and second resonance frequencies and jerk minimization[1]. Fig. 4 shows the frequency characteristic of $F_{\mathrm{m}}(z)$ designed for each stroke condition. From the figure, $F_{\mathrm{m}}(z)$ suppresses frequency components at around 2.9 kHz and 6.0 kHz for compensating for vibratory response owing to the vibration modes. Fig. 5 shows the time responses of the generated position trajectory reference r as the reference input in the 2DoF control system and model-based FF control input u_{mff}. As seen from Fig. 5, each position reference settles to the target position at the target settling time by the deadbeat control manner. If there are no modeling errors, the actual motor and mirror positions, y_{mot} and y_{mir}, can achieve the desired response by realizing $e_{\mathrm{mot}} = 0$ during the positioning motion with the model-based FF compensation. For details of the deadbeat FF control design method, see reference [3].

E. Undesired Error Response in Model-Based FF Compensation

We conducted positioning experiments on an actual galvano scanner to confirm the control performance of the model-based control approach. Here, it should be noted that the design of the model-based FF compensation used the design model obtained through curve fitting to the measured FRF, without any adjustment of model parameters for improving positioning performance. Fig. 6 shows the motor position y_{mot}, mirror position y_{mir}, and their position errors $Y_{\mathrm{r}} - y_{\mathrm{mot}}$ and $Y_{\mathrm{r}} - y_{\mathrm{mir}}$ for each stroke condition. As indicated in the position responses, from a macroscopic perspective, thanks to the model-based FF compensation,
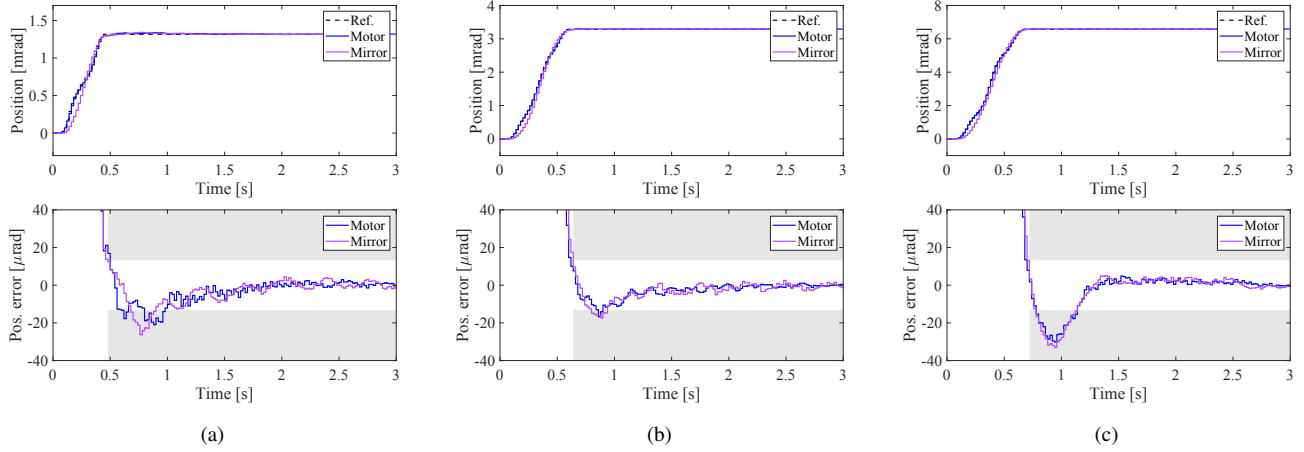
Fig. 6. Experimental waveforms of position, y_{mot} and y_{mir}, and position error, $Y_{\mathrm{r}} - y_{\mathrm{mot}}$ and $Y_{\mathrm{r}} - y_{\mathrm{mir}}$, in case of model-based FF compensation: (a) C1; (b) C2; (c) C3.

y_{mot} followed r with high accuracy, and both y_{mot} and y_{mir} rapidly settled to the target position. However, when we focused on the position errors, both y_{mot} and y_{mir} experienced an non-negligible overshoot immediately after settling, exceeding the target settling accuracy of ± 13.2 µrad in all stroke conditions.

The experimental results revealed that owing to the influence of minor modeling errors for nonlinear dynamics such as friction and identification errors in the FRF measurement, it was difficult to satisfy the control specifications using the model-based FF compensation designed via a general system identification method. As mentioned in Sect. I, in industry, engineers tune the model parameters and/or introduce the additive FF controller. In the following sections, we improved the positioning accuracy by applying DDC-based additive FF compensation supplementary to the existing model-based FF compensation with considerable effort to overcome this problem.

III. DATA-DRIVEN DESIGN THEORY OF ADDITIVE FF COMPENSATION

A. Objective Function

The additive FF controller $F_{\mathrm{a}}(z, \boldsymbol{\rho})$ in Fig. 3 is defined as a linear structure of the basis function vector $\boldsymbol{\Psi}(z) \in \mathbb{C}^{1 \times (N+1)}$ and parameter vector $\boldsymbol{\rho} \in \mathbb{R}^{N+1}$:

$$
\begin{aligned}
F_{\mathrm{a}}(z, \boldsymbol{\rho}) &= \boldsymbol{\Psi}(z) \boldsymbol{\rho} \\
\boldsymbol{\Psi}(z) &= [\Psi_0(z) \ \Psi_1(z) \ \cdots \ \Psi_N(z)] \\
\boldsymbol{\rho} &= [\rho_0 \ \rho_1 \ \cdots \ \rho_N]^{\top}
\end{aligned}
\tag{2}
$$

The design target, $\boldsymbol{\rho}$, is set by solving the optimization problem shown in (3) to minimize the error between the target position reference $r(t)$ and the predicted motor position $\hat{y}_{\mathrm{mot}}(t, \boldsymbol{\rho})$ at discrete time $t = M_{\mathrm{st}}, M_{\mathrm{st}} + 1, \ldots, M_{\mathrm{ed}}$.

$$
\mathcal{J}(\boldsymbol{\rho}) = \sum_{t=M_{\mathrm{st}}}^{M_{\mathrm{ed}}} (r(t) - \hat{y}_{\mathrm{mot}}(t, \boldsymbol{\rho}))^2
\tag{3}
$$

The noteworthy point in (3) is that in the proposed approach, the position reference r generated by the model-based FF control is directly used as the reference input to be followed in the design of DDC-based FF control.

First, if G is an LTI system with an SISO of $x(t)$ as input and $y(t)$ as output, the lifted representation at $t = 0, 1, \ldots, M_{\mathrm{ed}}$ is expressed as

$$
\boldsymbol{y} = \boldsymbol{G} \boldsymbol{x}
\tag{4}
$$

where

$$
\boldsymbol{G} = \begin{bmatrix}
D & 0 & \cdots & 0 \\
\boldsymbol{CB} & D & \cdots & 0 \\
\vdots & \vdots & \ddots & \vdots \\
\boldsymbol{CA}^{M_{\mathrm{ed}}-2}\boldsymbol{B} & \boldsymbol{CA}^{M_{\mathrm{ed}}-3}\boldsymbol{B} & \cdots & D
\end{bmatrix}
\tag{5}
$$

$$
\in \mathbb{R}^{(M_{\mathrm{ed}}+1) \times (M_{\mathrm{ed}}+1)}
$$

$$
\boldsymbol{y} = [y(0) \ y(1) \ \cdots \ y(M_{\mathrm{ed}})]^{\top} \in \mathbb{R}^{M_{\mathrm{ed}}+1}
$$

$$
\boldsymbol{x} = [x(0) \ x(1) \ \cdots \ x(M_{\mathrm{ed}})]^{\top} \in \mathbb{R}^{M_{\mathrm{ed}}+1}
$$

Note that $\boldsymbol{A}, \boldsymbol{B}, \boldsymbol{C}$, and D in the Toeplitz matrix $\boldsymbol{G}$ are coefficient matrices of G. Applying the above lifted expression to $P_{\mathrm{mot}}(z)$, $\tilde{P}_{\mathrm{mot}}(z)$, $\tilde{P}'_{\mathrm{mot}}(z)$, $C(z)$, and $F_{\mathrm{a}}(z)$, we can denote the Toeplitz matrices as $\boldsymbol{P}_{\mathrm{mot}}$, $\tilde{\boldsymbol{P}}_{\mathrm{mot}}$, $\tilde{\boldsymbol{P}}'_{\mathrm{mot}}$, $\boldsymbol{C}$, and $\boldsymbol{F}_{\mathrm{a}}$, respectively. Expressing $r(t)$, $u_{\mathrm{mff}}(t)$, and $\hat{y}_{\mathrm{mot}}$ as vectors in $t = 0, 1, \ldots, M_{\mathrm{ed}}$ gives

$$
\begin{aligned}
\boldsymbol{r} &= [r(0) \ r(1) \ \cdots \ r(M_{\mathrm{ed}})]^{\top} \in \mathbb{R}^{M_{\mathrm{ed}}+1} \\
\boldsymbol{u}_{\mathrm{mff}} &= [u_{\mathrm{mff}}(0) \ u_{\mathrm{mff}}(1) \ \cdots \ u_{\mathrm{mff}}(M_{\mathrm{ed}})]^{\top} \in \mathbb{R}^{M_{\mathrm{ed}}+1} \\
\hat{\boldsymbol{y}}_{\mathrm{mot}}(\boldsymbol{\rho}) &= [\hat{y}_{\mathrm{mot}}(0, \boldsymbol{\rho}) \ \hat{y}_{\mathrm{mot}}(1, \boldsymbol{\rho}) \\
&\qquad \cdots \ \hat{y}_{\mathrm{mot}}(M_{\mathrm{ed}}, \boldsymbol{\rho})]^{\top} \in \mathbb{R}^{M_{\mathrm{ed}}+1}
\end{aligned}
\tag{6}
$$

In this vector notation, $\hat{\boldsymbol{y}}_{\mathrm{mot}}(\boldsymbol{\rho})$ can be represented as follows:

$$
\begin{aligned}
\hat{\boldsymbol{y}}_{\mathrm{mot}}(\boldsymbol{\rho}) &= (\boldsymbol{I} + \boldsymbol{P}_{\mathrm{mot}}\boldsymbol{C})^{-1} \boldsymbol{P}_{\mathrm{mot}} \\
&\quad (\boldsymbol{I} + \boldsymbol{C}\tilde{\boldsymbol{P}}_{\mathrm{mot}} + \boldsymbol{F}_{\mathrm{a}}(\boldsymbol{\rho})\tilde{\boldsymbol{P}}'_{\mathrm{mot}})\boldsymbol{u}_{\mathrm{mff}}
\end{aligned}
\tag{7}
$$

However, $\hat{\boldsymbol{y}}_{\mathrm{mot}}(\boldsymbol{\rho})$ in (7) cannot directly predict the response as stated since it contains the unknown $\boldsymbol{P}_{\mathrm{mot}}$. Therefore,

based on the DDC approach[13], [14], [15], after conducting a learning data acquisition experiment with the initial parameter $\boldsymbol{\rho}_0$, we used the output response data $y_{\mathrm{mot0}}(t), t = 0, 1, \ldots, M_{\mathrm{ed}}$ to predict $\hat{\boldsymbol{y}}_{\mathrm{mot}}$ via an expression independent of $\boldsymbol{P}_{\mathrm{mot}}$. As in (7), it was assumed that the following equation holds for the vector $\boldsymbol{y}_{\mathrm{mot0}} \in \mathbb{R}^{M_{\mathrm{ed}}}$ of $y_{\mathrm{mot0}}(t)$ obtained from the learning experiment.

$$
\begin{aligned}
\boldsymbol{y}_{\mathrm{mot0}} &= [y_{\mathrm{mot0}}(0, \boldsymbol{\rho}_0) \; y_{\mathrm{mot0}}(1, \boldsymbol{\rho}_0) \; \cdots \; y_{\mathrm{mot0}}(M_{\mathrm{ed}}, \boldsymbol{\rho}_0)]^\top \\
&= (\boldsymbol{I} + \boldsymbol{P}_{\mathrm{mot}}\boldsymbol{C})^{-1}\boldsymbol{P}_{\mathrm{mot}} \\
&\quad (\boldsymbol{I} + \boldsymbol{C}\tilde{\boldsymbol{P}}_{\mathrm{mot}} + \boldsymbol{F}_{\mathrm{a}}(\boldsymbol{\rho}_0)\tilde{\boldsymbol{P}}'_{\mathrm{mot}})\boldsymbol{u}_{\mathrm{mff}}
\end{aligned}
\tag{8}
$$

When additive FF compensation is not applied, this corresponds to $\boldsymbol{F}_{\mathrm{a}}(\boldsymbol{\rho}_0) = \boldsymbol{O}$; therefore, (8) can be simplified as follows:

$$
\boldsymbol{y}_{\mathrm{mot0}} = (\boldsymbol{I} + \boldsymbol{P}_{\mathrm{mot}}\boldsymbol{C})^{-1}\boldsymbol{P}_{\mathrm{mot}}(\boldsymbol{I} + \boldsymbol{C}\tilde{\boldsymbol{P}}_{\mathrm{mot}})\boldsymbol{u}_{\mathrm{mff}} \tag{9}
$$

If $\boldsymbol{u}_{\mathrm{mff}}$ is removed by combining (7) and (9) and $\hat{\boldsymbol{y}}_{\mathrm{mot}}(\boldsymbol{\rho})$ is rearranged, $\hat{\boldsymbol{y}}_{\mathrm{mot}}(\boldsymbol{\rho})$ takes a form that does not include $\boldsymbol{P}_{\mathrm{mot}}$, as shown in the following equation:

$$
\begin{aligned}
\hat{\boldsymbol{y}}_{\mathrm{mot}}(\boldsymbol{\rho}) &= \boldsymbol{y}_{\mathrm{mot0}} + \boldsymbol{F}_{\mathrm{a}}(\boldsymbol{\rho})\boldsymbol{y}_{\mathrm{Smot0}} \\
\boldsymbol{y}_{\mathrm{Smot0}} &= \tilde{\boldsymbol{P}}'_{\mathrm{mot}}(\boldsymbol{I} + \boldsymbol{C}\tilde{\boldsymbol{P}}_{\mathrm{mot}})^{-1}\boldsymbol{y}_{\mathrm{mot0}}
\end{aligned}
\tag{10}
$$

Furthermore, considering (2), $\hat{\boldsymbol{y}}_{\mathrm{mot}}(\boldsymbol{\rho})$ can be expressed as an Affine function of $\boldsymbol{\rho}$:

$$
\begin{aligned}
\hat{\boldsymbol{y}}_{\mathrm{mot}}(\boldsymbol{\rho}) &= \boldsymbol{y}_{\mathrm{mot0}} + \boldsymbol{Q}\boldsymbol{\rho} \\
\boldsymbol{Q} &= [\boldsymbol{\Psi}_0\boldsymbol{y}_{\mathrm{Smot0}} \; \boldsymbol{\Psi}_1\boldsymbol{y}_{\mathrm{Smot0}} \; \cdots \; \boldsymbol{\Psi}_N\boldsymbol{y}_{\mathrm{Smot0}}] \\
&\quad \in \mathbb{R}^{(M_{\mathrm{ed}}+1)\times(N+1)}
\end{aligned}
\tag{11}
$$

where $\boldsymbol{\Psi}_i, i = 0, 1, \ldots, N$ are Toeplitz matrices corresponding to the basis function $\Psi_i(z)$. Equation (11) reveals that the prediction $\hat{\boldsymbol{y}}_{\mathrm{mot}}$ can be directly obtained from learning data $\boldsymbol{y}_{\mathrm{mot}}$.

From the above, the objective function $\mathcal{J}(\boldsymbol{\rho})$ in (3) can be expressed using $\boldsymbol{\rho}$:

$$
\begin{aligned}
\mathcal{J}(\boldsymbol{\rho}) &= \|\boldsymbol{V}(\boldsymbol{r} - \hat{\boldsymbol{y}}_{\mathrm{mot}}(\boldsymbol{\rho}))\|^2 \\
&= \|\boldsymbol{V}(\boldsymbol{e}_{\mathrm{mot0}} - \boldsymbol{Q}\boldsymbol{\rho})\|^2
\end{aligned}
\tag{12}
$$

with

$$
\begin{aligned}
\boldsymbol{e}_{\mathrm{mot0}} &= \boldsymbol{r} - \boldsymbol{y}_{\mathrm{mot0}} \in \mathbb{R}^{M_{\mathrm{ed}}+1} \\
\boldsymbol{V} &= \begin{bmatrix} \boldsymbol{O}_{M_{\mathrm{st}}\times(M_{\mathrm{ed}}+1)} \\ \boldsymbol{I}_{(M_{\mathrm{ed}}-M_{\mathrm{st}}+1)\times(M_{\mathrm{ed}}+1)} \end{bmatrix} \in \mathbb{R}^{(M_{\mathrm{ed}}+1)\times(M_{\mathrm{ed}}+1)}
\end{aligned}
\tag{13}
$$

where the symbol $\|\boldsymbol{y}\|$ represents the 2-norm of the vector $\boldsymbol{y}$.

B. Constraint

To design the augmented FF controller $F_{\mathrm{a}}(z, \boldsymbol{\rho})$ that outputs zeros after the deley-free position reference r' settles to a constant value, the following equality constraint is introduced:

$$
\begin{aligned}
F_{\mathrm{a}}(1, \boldsymbol{\rho}) &= \boldsymbol{\Sigma}\boldsymbol{\rho} = 0 \\
\boldsymbol{\Sigma} &= [1 \; 1 \; \cdots \; 1] \in \mathbb{R}^{1\times(N+1)}
\end{aligned}
\tag{14}
$$

C. Optimization Problem and Optimal Solution Calculation

By considering the objective function $\mathcal{J}(\boldsymbol{\rho})$ in (12) as a quadratic form of $\boldsymbol{\rho}$ and the equality constraint in (14) as an Affine function regarding $\boldsymbol{\rho}$, the optimization problem to design the additive FF controller is defined as follows:

$$
\begin{aligned}
\boldsymbol{\rho}^* &:= \arg \min_{\boldsymbol{\rho}} \mathcal{J}(\boldsymbol{\rho}) \\
&\text{s.t.} \quad F_{\mathrm{a}}(1, \boldsymbol{\rho}) = 0
\end{aligned}
\tag{15}
$$

The optimal solution $\boldsymbol{\rho}^*$ can be found using the Lagrange's multiplier method. Define a Lagragian function $\mathcal{L}(\boldsymbol{\rho})$ as a linear combination of the objective function and the equality constraint with an undetermined coefficient $2\lambda \in \mathbb{R}$:

$$
\begin{aligned}
\mathcal{L}(\boldsymbol{\rho}) &= \mathcal{J}(\boldsymbol{\rho}) + 2\lambda F_{\mathrm{a}}(1, \boldsymbol{\rho}) \\
&= \|\boldsymbol{V}(\boldsymbol{e}_{\mathrm{mot0}} - \boldsymbol{Q}\boldsymbol{\rho})\|^2 + 2\lambda\boldsymbol{\Sigma}\boldsymbol{\rho}
\end{aligned}
\tag{16}
$$

The partial deviation of $\mathcal{L}(\boldsymbol{\rho})$ can be expressed with $\boldsymbol{W} = \boldsymbol{V}\boldsymbol{Q} \in \mathbb{R}^{(M_{\mathrm{ed}}+1)\times(N+1)}$ as follows:

$$
\frac{\partial \mathcal{L}(\boldsymbol{\rho})}{\partial \boldsymbol{\rho}} = -2\boldsymbol{W}^\top\{\boldsymbol{V}(\boldsymbol{e}_{\mathrm{mot0}} - \boldsymbol{Q}\boldsymbol{\rho})\} + 2\lambda\boldsymbol{\Sigma}^\top \tag{17}
$$

At the optimal solution, $\partial\mathcal{L}(\boldsymbol{\rho})/\partial\boldsymbol{\rho} = \boldsymbol{O}$ holds. Therefore, from (17), if $\boldsymbol{W}^\top\boldsymbol{W} \neq \boldsymbol{O}$, then $\boldsymbol{\rho}^*$ can be expressed using λ as

$$
\boldsymbol{\rho}^* = (\boldsymbol{W}^\top\boldsymbol{W})^{-1}(\boldsymbol{W}^\top\boldsymbol{V}\boldsymbol{e}_{\mathrm{mot0}} - \lambda\boldsymbol{\Sigma}^\top) \tag{18}
$$

Furthermore, from $\boldsymbol{\Sigma}\boldsymbol{\rho} = 0$ and (18), λ can be derived by

$$
\lambda = \{\boldsymbol{\Sigma}(\boldsymbol{W}^\top\boldsymbol{W})^{-1}\boldsymbol{\Sigma}^\top\}^{-1}\boldsymbol{\Sigma}(\boldsymbol{W}^\top\boldsymbol{W})^{-1}\boldsymbol{W}^\top\boldsymbol{V}\boldsymbol{e}_{\mathrm{mot0}} \tag{19}
$$

From (18) and (19), $\boldsymbol{\rho}^*$ can be calculated as follows:

$$
\begin{aligned}
\boldsymbol{\rho}^* = (\boldsymbol{W}^\top\boldsymbol{W})^{-1} \big[&\boldsymbol{W}^\top\boldsymbol{V}\boldsymbol{e}_{\mathrm{mot0}} \\
&-\boldsymbol{\Sigma}^\top\{\boldsymbol{\Sigma}(\boldsymbol{W}^\top\boldsymbol{W})^{-1}\boldsymbol{\Sigma}^\top\}^{-1} \\
&\boldsymbol{\Sigma}(\boldsymbol{W}^\top\boldsymbol{W})^{-1}\boldsymbol{W}^\top\boldsymbol{V}\boldsymbol{e}_{\mathrm{mot0}} \big]
\end{aligned}
\tag{20}
$$

From the above design theory, we can design the additive FF controller based on a data-driven approach directly using learning data $\boldsymbol{r}$ and $\boldsymbol{y}_{\mathrm{mot}}$ obtained through a single operating experiment. Furthermore, by combining with the model-based FF compensation, a reference model is not necessary.

IV. EXPERIMENTAL EVALUATION

To overcome the problems of model-based FF compensation described in Sect. II, we next applied the DDC-based additive FF compensation presented in Sect. III and evaluated its effectiveness experimentally.

A. Design of Augmented FF Controller

For the additive FF controller $F_{\mathrm{a}}(z, \boldsymbol{\rho})$ in this study, we used the FIR-type controller represented in the following equation, considering flexibility in terms of compensating for unknown modeling errors[20]:

$$
F_{\mathrm{a}}(z, \boldsymbol{\rho}) = \boldsymbol{\Psi}(z)\boldsymbol{\rho} = \begin{bmatrix} 1 & z^{-1} & \cdots & z^{-N} \end{bmatrix} \begin{bmatrix} \rho_0 \\ \rho_1 \\ \vdots \\ \rho_N \end{bmatrix} \tag{21}
$$

TABLE III

Condition	M_{st}	M_{ed}
C1	24 (0.48 ms)	124 (2.48 ms)
C2	32 (0.64 ms)	132 (2.64 ms)
C3	36 (0.72 ms)	136 (2.72 ms)
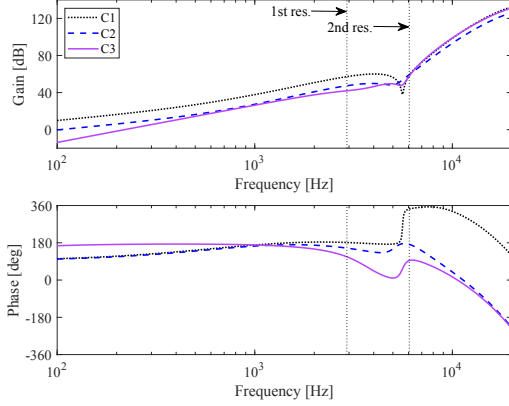
Fig. 7. Frequency characteristics of additive FF controller $F_a(z)$.

Fig. 8. Waveforms of additive FF control input u_{aff}.

The order N was manually set to $N = 7$, providing an adequate degree of freedom for the improvement of control performance. The parameter ρ in (21) was designed based on (20) for each stroke condition. Here, the learning data r and y_{mot0} were measured in the corresponding stroke condition using the existing model-based FF compensation shown in Fig. 6. To set the evaluation time interval of the predicted response evaluation to 2.00 ms after the target settling time, we set M_{st} and M_{ed} as shown in Table III.

Fig. 7 shows the frequency characteristics of the additive FF controller $F_a(z)$. While the designed controllers fundamentally possess similar derivative properties, they exhibit characteristics with varying gains and phases depending on the stroke conditions. In the model-based control approach, in general, fine-tune of the controllers for various operating conditions necessitates considerable effort; however, the proposed DDC approach can design the appropriate controllers efficiently only by conducting a learning data acquisition experiment. Fig. 8 shows the additive FF control input u_{aff}. The designed controllers output stable control inputs during the transient response of positioning operations, and zeros in the steady state.

B. Results of Positioning Experiment

Fig. 9 shows the response waveforms of the motor position y_{mot}, the mirror position y_{mir}, and their position error $Y_r - y_{mot}$ and $Y_r - y_{mir}$ from the positioning experiments when the additive FF compensation was applied. From the figure, for all stroke conditions, the undesired overshoot after settling were significantly suppressed, compared to the results shown in Fig. 6, and both motor and mirror responses satisfied the target settling accuracy of ± 13.2 μm within the target settling times. In terms of quantitative evaluation,
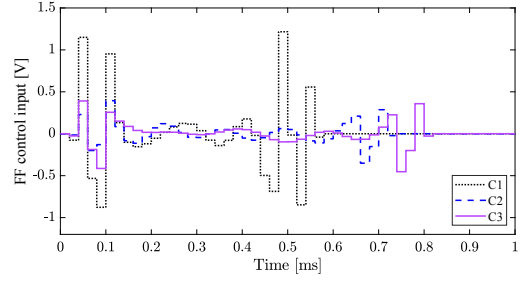
Table IV shows the RMS of the position error and the settling time of the motor and mirror positions for the 2.00 ms interval following each target settling time. The additive FF compensation significantly reduced the RMS of the error and shortened the settling time for the motor and mirror, resulting in the improvement of fast and precise positioning performance.

C. Consideration of Error Response Suppression Mechanism

To investigate the mechanism of the error response suppression owing to the additive FF compensation, we analyzed the position tracking responses of the motor during the positioning operation between without and with additive FF compensation. Fig. 10 shows the time response waveform and frequency spectrum of the motor position tracking error e_{mot}. In the absence of the additive FF compensation, the error responses that caused overshoot after the settling occurred during the transient response of the point-to-point motion, and their frequency components were mainly between 500 Hz and 1.2 kHz below the response frequencies. In contrast, when additive FF compensation was applied, the additive FF control input u_{aff} shown in Fig. 8 reduced low-frequency tracking errors, particularly in the frequency range of 500 Hz to 1.2 kHz, thereby suppressing overshoot at the settling.

Next, Fig. 11 shows the predicted waveforms of the motor position error $Y_r - \hat{y}_{mot}$ calculated using (11) with the optimal parameter ρ^* in the case with the additive FF compensation. The proposed data-driven method accurately predicted the measured actual response, and the performance improvement from the model-based FF compensation is similar to the experimental results shown in Fig. 6 and Fig. 9. Therefore, it is evident that the proposed method designs additive FF controllers shown in Fig. 7 to suppress undesired error responses through accurate response prediction driven by learning data and control cost optimization regarding the predicted response.

V. CONCLUSION

In this study, we proposed a DDC-based design method for additive FF compensation aimed at fast and precise control of industrial positioning mechanisms. The proposed method enabled efficient controller design by directly predicting responses from learning data obtained from a single positioning experiment and optimizing the predicted response.
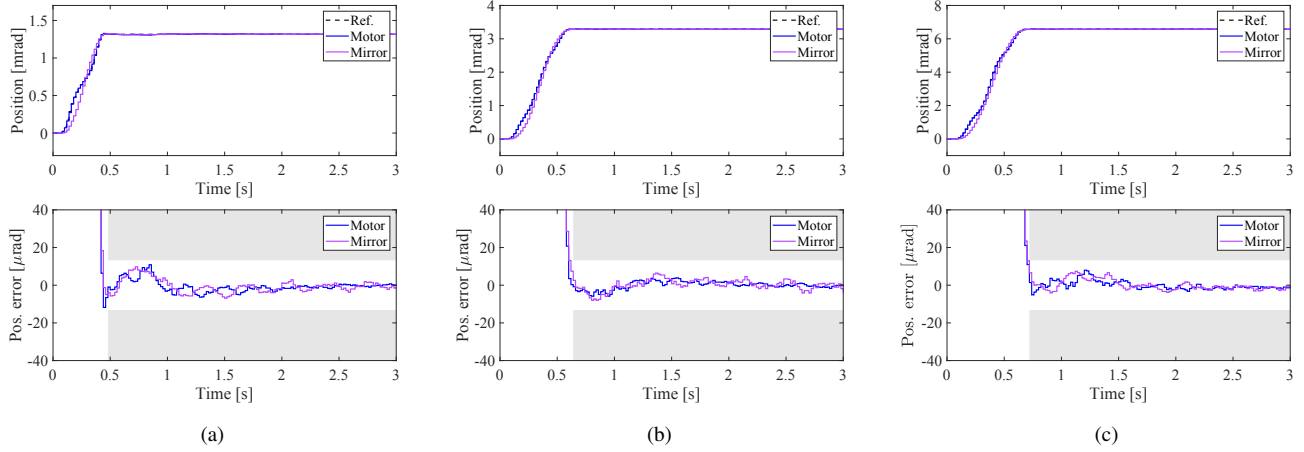
Fig. 9. Experimental waveforms of position, y_{mot} and y_{mir}, and position error, $Y_{\mathrm{r}} - y_{\mathrm{mot}}$ and $Y_{\mathrm{r}} - y_{\mathrm{mir}}$, in case of additive FF compensation: (a) C1; (b) C2; (c) C3.

TABLE IV
COMPARISON OF POSITIONING PERFORMANCE.

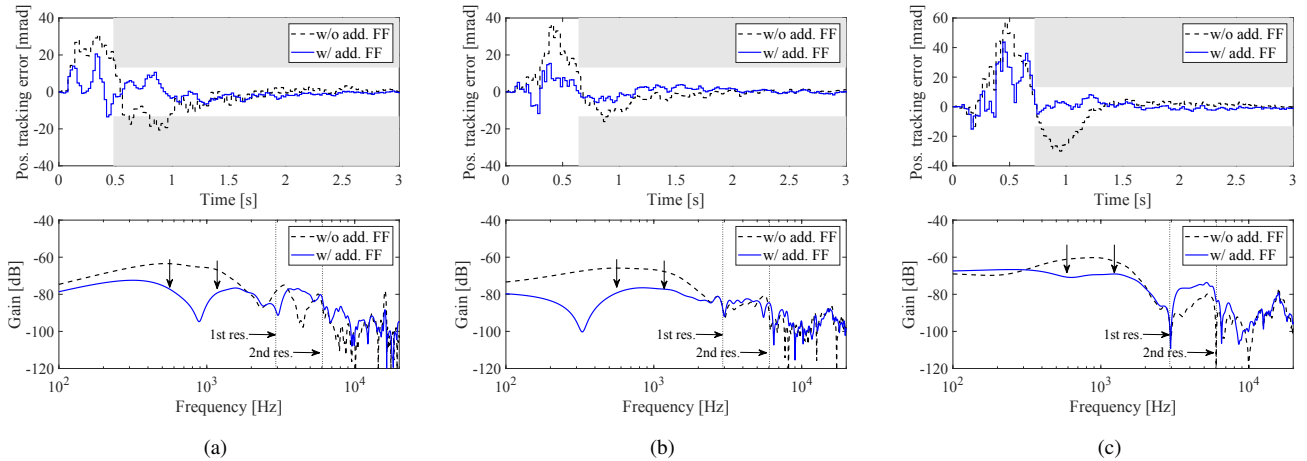| Condition | Additive FF | RMS of pos. error [μrad] | | Settling time [ms] | |
		Motor	Mirror	Motor	Mirror
C1	w/o	8.84	8.65	0.98	0.90
	w/	3.49 (−60.5 %)	3.92 (−54.7 %)	0.42 (−57.1 %)	0.44 (−51.1 %)
C2	w/o	5.27	6.06	0.90	0.94
	w/	2.24 (−57.5 %)	3.08 (−49.2 %)	0.60 (−33.3 %)	0.62 (−34.0 %)
C3	w/o	10.20	11.20	1.14	1.14
	w/	2.60 (−74.5 %)	3.13 (−72.1 %)	0.70 (−38.6 %)	0.70 (−38.6 %)

Fig. 10. Time response waveform and frequency spectrum of motor position tracking error e_{mot} in cases without/with additive FF compensation: (a) C1; (b) C2; (c) C3.

By applying the proposed additive FF compensation in conjunction with the existing model-based FF compensation, it enabled to effectively compensate for undesirable responses caused by unknown modeling errors that were not adequately suppressed by the traditional model-based control approach. The practical effectiveness of the proposed approach has been verified through positioning experiments using a galvano scanner under multiple stroke conditions, enabling the attainment of the target control specifications with a significant improvement in positioning accuracy.

REFERENCES

[1] M. Iwasaki, K. Seki, and Y. Maeda, "High-Precision Motion Control Techniques: A Promising Approach to Improving Motion Performance," *IEEE Ind. Electron. Mag.*, Vol. 6, No. 1, pp. 32–40, 2012.
[2] R. de Rozario, A. Fleming, and T. Oomen, "Finite-Time Learning Control Using Frequency Response Data With Application to a Nanopositioning Stage," *IEEE/ASME Trans. Mechatron.*, Vol. 24, No. 5, pp. 2085–2096, 2019.
[3] Y. Maeda and M. Iwasaki, "Improvement of Adaptive Property by Adaptive Deadbeat Feedforward Compensation Without Convex Optimization," *IEEE Trans. Ind. Electron.*, Vol. 62, No. 1, pp. 466–474, 2015.
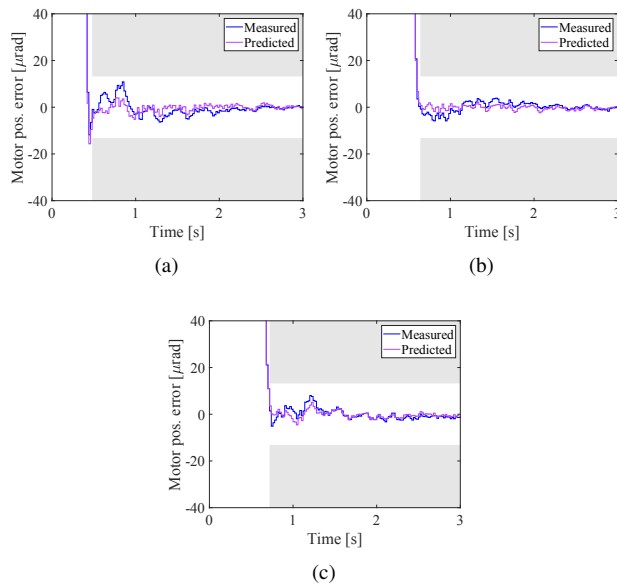
Fig. 11. Waveforms of predicted motor position error $Y_r - \hat{y}_{\mathrm{mot}}$ in case of additive FF compensation with optimal parameter: (a) C1; (b) C2; (c) C3.

[4] J. Schoukens, K. Godfrey, and M. Schoukens, "Nonparametric Data-Driven Modeling of Linear Systems," *IEEE Control Sys. Mag.*, Vol. 38, No. 4, pp. 49–88, 2018.

[5] W. Zhou and J. Beerten, "Extrapolation of Band-Limited Frequency Responses for Out-of-Band Modal Synthesis," *Proc. Int. Power Electron. Conf.*, pp. 1578–1583, 2022.

[6] T. Semba and M.T. White, "Seek Control to Suppress Vibrations of Hard Disk Drives Using Adaptive Filtering" *IEEE/ASME Trans. Mechatron.*, Vol. 13, No. 5, pp. 502–509, 2008.

[7] F. Boeren, D. Bruijnen, N. van Dijk, T. Oomen, "Joint Input Shaping and Feedforward for Point-To-Point Motion: Automated Tuning for an Industrial Nanopositioning System," *Mechatronics*, Vol. 24, No. 6, pp. 572–581, 2014.

[8] C.-W. Ha and D. Lee, "Analysis of Embedded Prefilters in Motion Profiles," *IEEE Trans. Ind. Electron.*, Vol. 65, No. 2, pp. 1481–1489, 2018.

[9] F. Dörfler, "Data-Driven Control: Part One of Two: A Special Issue Sampling from a Vast and Dynamic Landscape" *IEEE Control Syst. Mag.*, Vol. 43, No. 5, pp. 24–27, 2023.

[10] F. Dörfler, "Data-Driven Control: Part Two of Two: Hot Take: Why not go with Models?" *IEEE Control Syst. Mag.*, Vol. 43, No. 6, pp. 27–31, 2023.

[11] M.C. Campi, A. Lecchini, and S.M. Savaresi, "Virtual reference feedback tuning: a direct method for the design of feedback controllers," *Automatica*, Vol. 38, pp. 1337–1346, 2002.

[12] S. Formentin, P.D. Filippi, M. Corno, M. Tanelli, and S.M. Savaresi, "Data-Driven Design of Braking Control Systems," *IEEE Trans. Contr. Syst. Tech.*, Vol. 21, No. 1, pp. 186–193, 2013.

[13] O. Kaneko and T. Nakamura, "Data-Driven Prediction of 2DOF Control Systems with Updated Feedforward Controller," in *Proc. SICE Annu. Conf. 2017*, pp. 259–262, 2017.

[14] Y. Fujimoto, "Estimated Response Iterative Tuning with Signal Projection," *IFAC Journal Syst. Contr.*, Vol. 19, 8 pages, 2022.

[15] S. Ishihara, "Designing Reference Model for Estimated Response Iterative Tuning by Preference Learning," in *Proc. IEEE 28th Int. Conf. Emerging Tech. Factory Autom.*, 6 pages, 2023.

[16] V. Breschi and S. Formentin, "AutoDDC: Hyperparameter Tuning for Direct Data-Driven Control," *IEEE Control Syst. Mag.*, Vol. 43, No. 6, pp. 98–124, 2023.

[17] Y. Maeda and M. Iwasaki, "Empirical Transfer Function Estimation with Differential Filtering and Its Application to Fine Positioning Control of Galvano Scanner," *IEEE Trans. Ind. Electron.*, Vol. 70, No. 10, pp. 10466–10475, 2023.

[18] B. Gustavsen and A. Semlyen, "Rational Approximation of Frequency Domain Responses by Vector Fitting," *IEEE Trans. Power Del.*, Vol. 14, No. 3, pp. 1052–1061, 1999.

[19] E. Kuroda, Y. Maeda, and M. Iwasaki, "Autonomous Parameter Design for Cascade-Structure Feedback Controller Based on Cooperative Optimization Method," *IEEJ J. Ind. App.*, Vol. 10, No. 4, pp. 457–468, 2021.

[20] L. Dai, X. Li, Y. Zhu, M. Zhang, and C. Hu, "The Generation Mechanism of Tracking Error During Acceleration or Deceleration Phase in Ultraprecision Motion Systems," *IEEE Trans. Ind. Electron.*, Vol. 66, No. 9, pp. 7109–7119, 2019.